

# The Effects of Different Input Excitation on the Dynamic Characterization of an Automotive Shock Absorber

**Darin Kowalski, Mohan D. Rao**

Michigan Technological University, Houghton MI 49931

**Jason Blough, Scott Gruenberg**

Keweenaw Research Center, Michigan Technological University, Houghton MI 49931

**Dave Griffiths**

Ford Motor Company, Dearborn MI 48121

Copyright © 2001 Society of Automotive Engineers, Inc.

## ABSTRACT

This paper deals with the dynamic characterization of an automotive shock absorber, a continuation of an earlier work [1]. The objective of this on-going research is to develop a testing and analysis methodology for obtaining dynamic properties of automotive shock absorbers for use in CAE-NVH low-to-mid frequency chassis models. First, the effects of temperature and nominal length on the stiffness and damping of the shock absorber are studied and their importance in the development of a standard test method discussed. The effects of different types of input excitation on the dynamic properties of the shock absorber are then examined. Stepped sine sweep excitation is currently used in industry to obtain shock absorber parameters along with their frequency and amplitude dependence. Sine-on-sine testing, which involves excitation using two different sine waves has been done in this study to understand the effects of the presence of multiple sine waves on the estimated dynamic properties. In an effort to obtain all frequency dependent parameters simultaneously, different types of broadband random excitations have been studied. Results are compared with stepped sine sweep tests. Additionally, actual road data measured on different road profiles has been used as input excitation to obtain the shock absorber parameters for broad frequency bands under realistic amplitude and frequency conditions. These results are compared with both simulated random excitation and stepped sine sweep test results.

## INTRODUCTION

The shock absorber is one of the most important elements in a vehicle suspension system. It is also one of the most non-linear and complex elements to model. The current method of characterizing the dynamic properties of shock absorbers for CAE models involves testing at discrete frequencies, displacements, and pre-loads using an MTS test machine. The dynamic stiffness (K) and damping (C) are extracted by fitting a linear model of the form  $F(\omega)=K*x(\omega)+C*v(\omega)$  to the measured input displacement (x), velocity (v), and output force (F). The excitation technique is a pure sine excitation at the desired frequency and amplitude. These harmonic excitations are then swept through all desired frequency and amplitudes.

Parametric and non-parametric models also exist for the shock absorber. A non-parametric model based on a restoring force surface mapping has been developed [2,3,4]. The model considers the force to be a function of displacement and velocity. Although, this model is more applicable to a single frequency excitation, it serves as a useful tool for identifying the non-linearity's in the system.

A comprehensive physical model was developed by Lang [5], later condensed and validated by Morman [6]. Lang's model has more than 80 parameters, is computationally complex and is not suitable for comprehensive vehicle simulation studies. Morman's model has been shown to be useful for studying the effects of design changes for a particular shock. Reybrouck [7] has developed a physical model, which has 14 parameters, valid for frequencies up to 20 Hz, but has limited appeal for the analysis of shock absorbers for NVH applications.

The goal of this study was to determine if the current excitation technique holds true when more than one frequency is present. The first task included standardizing the testing procedure. This is done because shock absorbers characteristics change with temperature and nominal length. Sine-on-sine testing, different types of broadband random excitations have been utilized. Results are compared with stepped sine sweep tests. Additionally, actual road data has been used as input excitation to obtain the shock absorber parameters for broad frequency bands under realistic amplitude and frequency conditions. Details of these are presented in the following sections

## TEST PROCEDURE

All of the testing for this project was done using the MTS 831 elastomer characterization machine located at the Keweenaw Research Center of Michigan Technological University. A picture of a shock absorber in the test fixture is shown in Figure 1. The hardware used to control the MTS 831 was TestStar II. In conjunction with TestStar II, TestWare-SX software was used to organize a test matrix and also to monitor and record the desired parameters throughout the test. TestWare-SX, however, is only capable of producing pure sine excitations. Therefore, Component RPCIII (CRPC) software was used to excite the test specimen with arbitrary time domain excitation. CRPC has the ability to generate pure sine waves, multiple sine waves, shaped random excitations, or any arbitrary time domain excitation.



Figure 1: MTS 831 Machine with Shock Absorber Installed

**ANALYSIS** - The analysis methodology that TestWare-SX uses in its stepped sine sweep is visualized in Figure 2 [8]. Shown in the figure are the output force vector ( $A_{load}$ ) and input displacement vector ( $A_{disp}$ ) plotted in a real and imaginary format. From this representation the stiffness ( $K$ ) and damping ( $C$ ) parameters can be

calculated. 
$$K^* = \frac{A_{load}}{A_{disp}}, \quad \Phi = \Phi_{load} - \Phi_{disp},$$

$$K = K^* \cos(\Phi), \text{ and } C = \frac{K^*}{\omega} \sin(\Phi).$$

This analysis method can be extended to all frequencies by realizing that  $K^*$  and  $\phi$  are simply the magnitude and phase of the frequency response function between the output force and input displacement. This analysis method is the current industry standard in the elastomer characterization. Therefore, it will be used to analyze all the new excitation methods presented in this paper.

## VALIDATION OF COMPONENT RPCIII – TestWare-SX

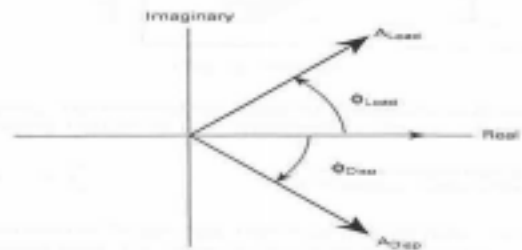


Figure 2: Force and Displacement Vectors

is assumed to yield correct shock absorber parameter estimates, since it is currently the defacto industry standard. Both CRPCIII and TestWare-SX are capable of producing pure sine wave input excitations. For this reason TestWare-SX has been used to validate CRPCIII for pure sine wave input excitations. The frequencies of interest are between 5 and 140 Hz. Figures 3 and 4 show that the estimates for the stiffness and damping parameters,  $K$  and  $C$ , are quite comparable between the two software packages. The reason for the slight deviation between the two is due to the fact that these estimates are not taken from the same data set. The same data set cannot be recorded by both software packages simultaneously, this results in a slight difference between data sets. Having validated the CRPC package, all further results presented in this paper have been obtained with the CRPC approach.

**TEMPERATURE EFFECTS** - It is widely know that shock absorber characteristics vary with temperature [9]. In an effort to eliminate temperature effects from the rest of this study, the shock absorber was instrumented with a thermocouple located on the outside of the main body of the shock absorber. The shock was then excited at 80 Hz and zero to peak amplitude of .85 mm for 32 minutes. The temperature, input displacement, and output force were recorded. Temperature and output force versus time is shown in Figure 5. It is clearly seen that the output force decreases as temperature increases. Since the input displacement was held constant,  $K^*$  decreases with temperature, as shown in Figure 6. It was determined that temperature would be

maintained between 75 and 80 °F for all future tests in order to limit errors due to temperature effects. To verify this, the temperature was monitored and recorded in all subsequent tests.

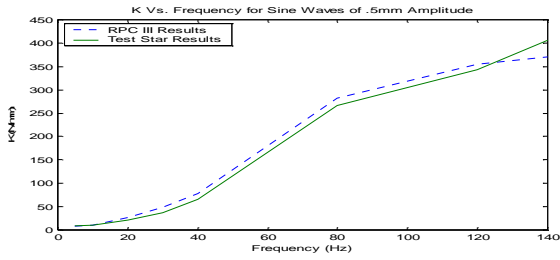


Figure 3: Stiffness Estimates from Test Star II and CRPCIII

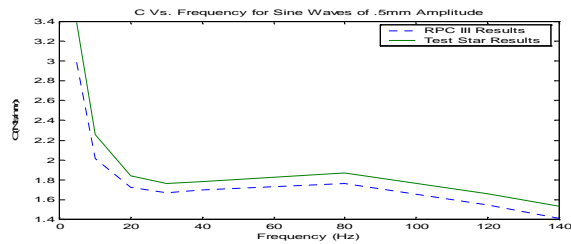


Figure 4: Damping Estimates from CRPCIII and Test Star II

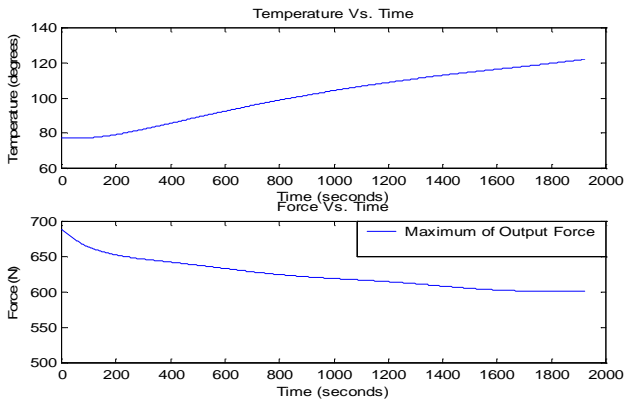


Figure 5: Output Force and Temperature for Temp Test

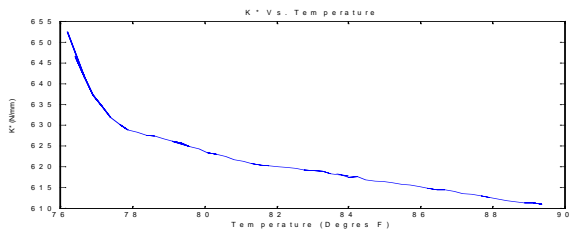


Figure 6: Variation of Dynamic Stiffness with Temperature

**NOMINAL LENGTH EFFECTS** - The nominal length of a shock absorber is defined here as the distance between the top of the shock body and the top of the piston rod, as shown in Figure 7.

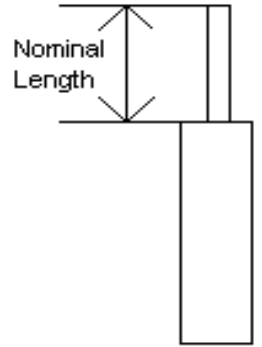


Figure 7: Nominal Length

The standard nominal length of this particular shock absorber was 110mm. To determine the effects of nominal length on the estimated shock absorber parameters, sine excitations of 20 and 120 Hz with zero to peak amplitudes of .5 mm were used at nominal lengths of 90, 100, 110, and 120 mm. The estimated parameters from these tests are shown in Figure 8. It can be seen that the estimated parameters are effected by the change in nominal length. The exact effect, however, is difficult to determine from such a small test matrix. This is because the 20 Hz stiffness estimations are effected differently than the 120 Hz stiffness estimations, as the nominal length is changed. Due to the dependency of the estimated shock absorber parameters on nominal length, the nominal length was checked to ensure that it was at the standard length in all remaining tests.

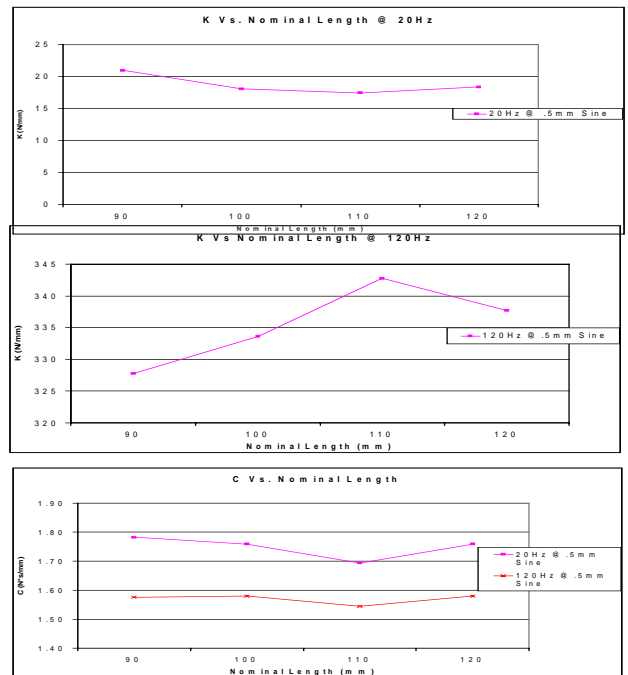


Figure 8: Results of K and C from Nominal Length Study

**PURE SINE SWEEP TESTS**

In order to understand the effects of multiple sine waves on K and C, a baseline for the shock absorber parameters was first established. The baseline consisted of pure sine waves with zero to peak amplitudes of .1, .25, .35, and .5 mm. The frequencies chosen for the pure sine waves were 5, 10, 20, 30, 40, 80, 120, and 140 Hz. The maximum frequency anti-alias

filter on the CRPC III boards is 160 Hz; therefore, the upper frequency limit was below this to eliminate possible filter effects. The force transducer established the lower frequency limit on the MTS 831, which was determined to be approximately 4 Hz. The results of the baseline testing are shown in Figures 9 and 10. It can clearly be seen that stiffness increases as a function of frequency. However, no clear trend emerged for stiffness as a function of amplitude. Figure 10 shows that the damping estimates decrease significantly as a function of frequency and amplitude at frequencies below 80 Hz. Above 80 Hz damping does not appear to change much with an increase in frequency.

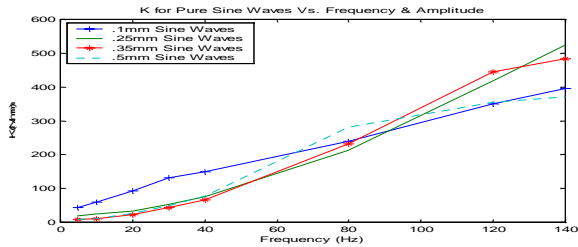


Figure 9: Stiffness Vs. Frequency Curves for Different Amplitudes

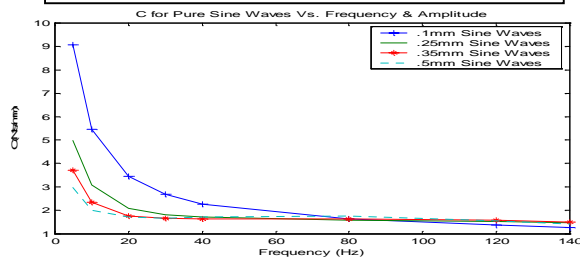


Figure 10: Damping Vs. Frequency Curves for Different Amplitudes

## SINE-ON-SINE EXCITATION

Having established the baseline, this study focussed on how these parameters change when two frequencies are present simultaneously. The driving force for this inquiry is that in practice, shock absorbers experience multiple frequencies simultaneously. Before the shock can be studied with many frequency inputs it must first be understood for two frequencies. The hypothesis is that when a higher frequency wave is superimposed on a lower frequency wave, the lower frequency wave breaks the static stiction of the shock resulting in a lower force requirement to move the shock at the higher frequency. Therefore, a lower stiffness estimate would be obtained at the higher frequency. An example of a sine-on-sine input is shown in Figure 11. It can be seen that the lower frequency higher amplitude wave looks like it is carrying the higher frequency lower amplitude wave. For this reason, the lower frequency wave is referred to as

the carrier wave and the higher frequency wave is referred to as the rider wave.

In order to understand this sine-on-sine excitation a test

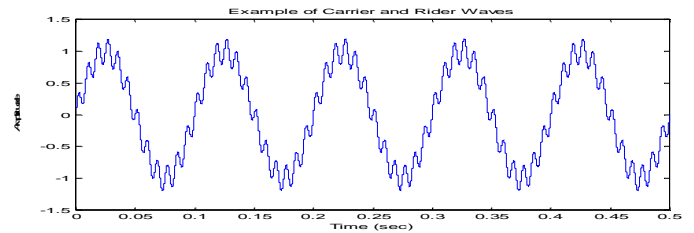


Figure 11: Example of Combined Carrier and Rider Wave

matrix was determined as follows. The frequencies of 5, 10, 20, and 30 Hz are the carrier wave frequencies. These frequencies were held at a constant amplitude of .5mm. The frequencies of 40, 80, 120, and 140 Hz are the rider frequencies. These frequencies will be added to the carrier wave frequencies at amplitudes of .1, .25, .35, and .5 mm. In summary, this results in four different rider frequencies at four distinct amplitudes being added to each of the four different carrier wave frequencies. This results in a total of 64 different test conditions.

**STIFFNESS ESTIMATES OF RIDER WAVES** - Shown in Figures 12-15 are the results that the carrier wave frequencies have on the rider wave stiffness estimates. Each graph is for a rider wave amplitude and has plotted the rider wave stiffness estimates versus frequency. Each series on these plots is for a different carrier wave frequency. Also plotted are the values of stiffness, at the appropriate amplitude, for the rider waves as pure sine inputs. When the rider amplitude is .1mm the variance on the estimations is the greatest. This is believed to be due to the fact that .1mm amplitudes are approaching the noise floor of the measurement system. At all of the higher amplitude rider waves the variance is less. The stiffness estimates at the rider wave frequencies seem to be independent of both the frequency of the carrier wave and the existence of a carrier wave. In conclusion, the existence of a carrier wave has little effect on the estimates of stiffness at the rider wave frequencies.

**DAMPING ESTIMATES OF RIDER WAVES** - Figures 16-19 show these results. The damping estimates below 100 Hz, for the rider frequencies, do not approximate the pure sine estimates as closely as the stiffness estimates did. However, above 100 Hz the rider wave damping estimates obtained with sine-on-sine input are approximately the same as the estimates obtained using pure sine input excitation. Another interesting result shown in these figures is that the damping estimates increase relative to the pure sine estimates, as the rider wave amplitude increases. Hence, at the lower amplitude rider waves the pure sine estimate is the highest estimate, and at the higher amplitude rider waves the pure sine estimate is the lowest estimate.

## STIFFNESS ESTIMATES OF CARRIER WAVES -

Plotted in Figures 20-23 are the results for stiffness estimates for the carrier waves. These plots are shown in the same manner as the rider wave results. Each graph is for one rider wave amplitude. Each series on these graphs is for a single rider wave frequency. It can be seen that the stiffness estimates for the carrier waves are effected by the presence of a rider wave. With the exceptions of carrier waves of 20 and 30 Hz, with a rider wave frequency of 40 Hz and amplitude .5mm, all of the carrier wave stiffness estimates are below the pure sine stiffness estimates. These graphs also show that the stiffness estimates for the carrier waves decrease as the rider frequency is increased. This is clearly evident in Figure 23 where the amplitudes of the rider and carrier waves are equal. Following the 140 Hz rider wave through all the amplitudes shows that the carrier wave stiffness estimates decrease as the rider amplitude increases. This trend is clearly evident when the 140 Hz rider amplitude is equal to the carrier amplitudes, because the stiffness of the carrier waves approach zero.

**DAMPING ESTIMATES OF CARRIER WAVES -** Figures 24-27 show the damping estimates for the carrier waves as a function of frequency. When comparing the damping results of the carrier waves to the damping results of the rider waves, the carrier wave estimates are effected greater than the rider estimates. The estimates are quite scattered with no clear trend emerging.

**CONCLUSIONS FROM SINE-ON-SINE TESTING -** The overall outcome of adding two sine waves together is difficult to sort out. However, the estimates at higher frequency waves are far less effected by the presence of the lower frequency wave than the opposite. This is evident by the stiffness estimates for the higher frequency waves falling much closer to the values obtained with pure sine inputs. It is also demonstrated by the damping estimate, which was much closer to the pure sine value for the higher frequency waves. In general, the higher frequency wave dominates the parameter estimates for the shock absorber. This is demonstrated by the highest frequency rider wave, of 140 Hz, at the largest amplitude of .5mm. When this wave was added to the lower frequency carrier waves the parameters estimated at 140 Hz were almost the same as the 140 Hz pure sine wave. While, the parameters estimated at the lower carrier frequencies tend towards zero. These results have yielded little light on what may happen when many frequencies are added together and the shock absorber characterized for all frequencies simultaneously. However, due to the rider wave dominance, it is speculated that the higher frequencies will hold closer towards the pure sine values while the lower frequencies tend towards zero.

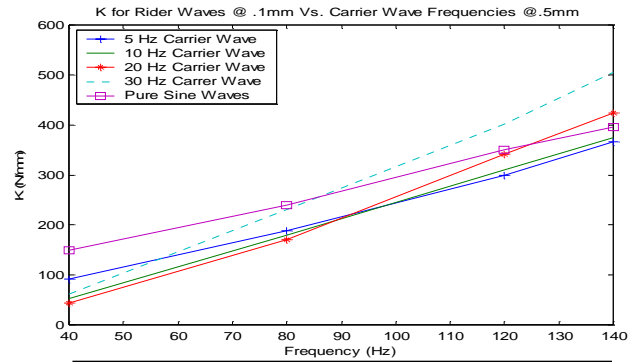


Figure 12: Effect of Carrier Wave Frequency on .1mm Rider Wave Stiffness Estimates

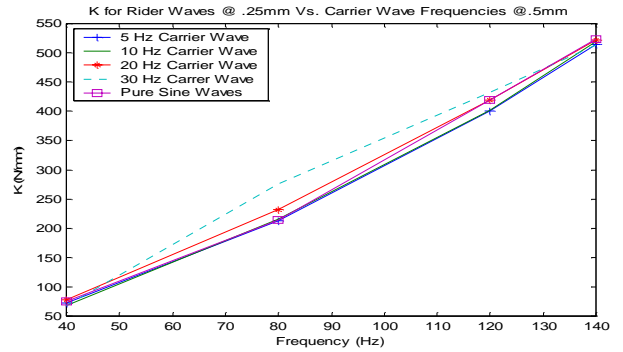


Figure 13: Effect of Carrier Wave Frequency on .25mm Rider Wave Stiffness Estimates

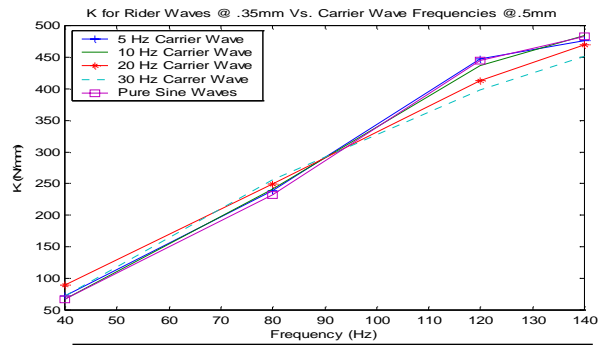


Figure 14: Effect of Carrier Wave Frequency on .35mm Rider Wave Stiffness Estimates

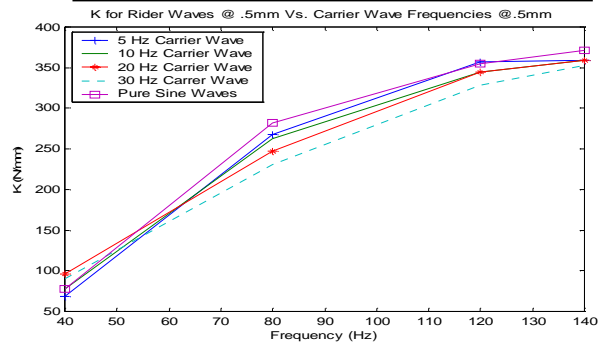


Figure 15: Effect of Carrier Wave Frequency on .5mm Rider Wave Stiffness Estimates

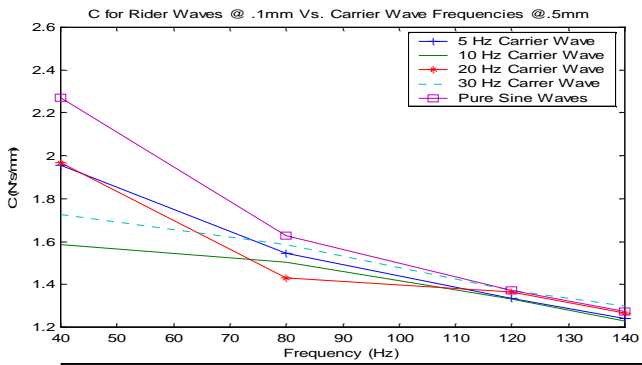


Figure 16: Effect of Carrier Wave Frequency on .1mm Rider Wave Damping Estimates

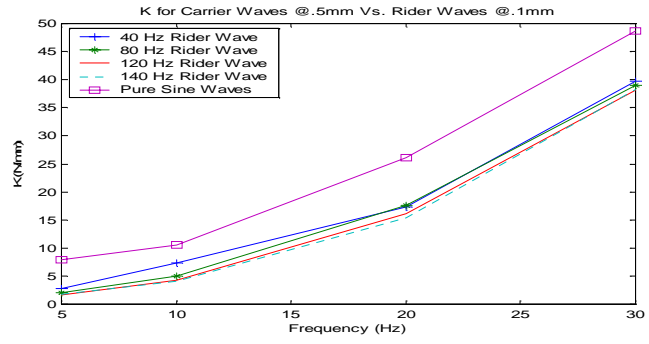


Figure 20: Effect of .1mm Rider Waves on Carrier Wave Stiffness Estimates

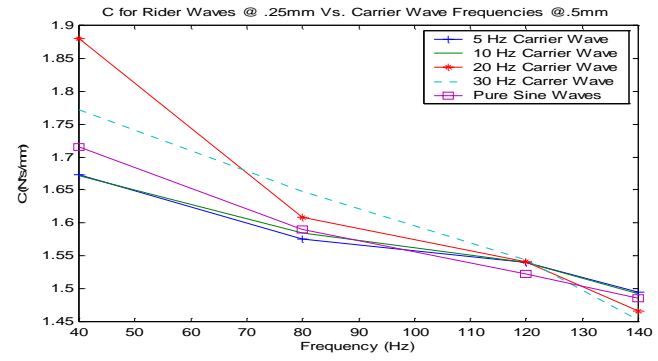


Figure 17: Effect of Carrier Wave Frequency on .25mm Rider Wave Damping Estimates

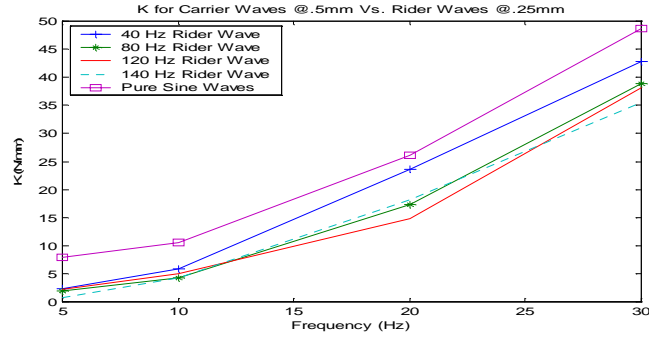


Figure 21: Effect of .25mm Rider Waves on Carrier Wave Stiffness Estimates

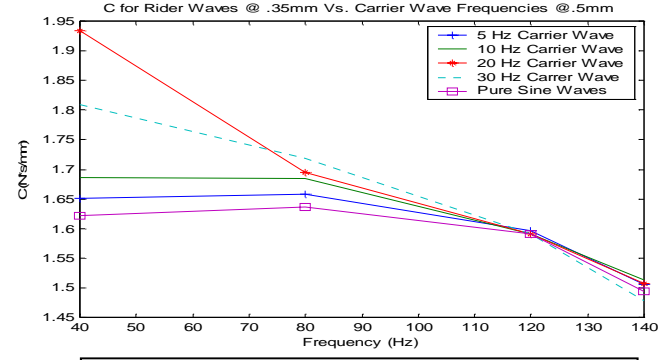


Figure 18: Effect of Carrier Wave Frequency on .35mm Rider Wave Damping Estimates

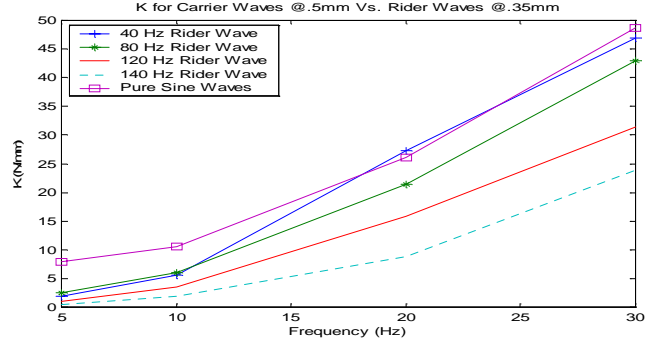


Figure 22: Effect of .35mm Rider Waves on Carrier Wave Stiffness Estimates

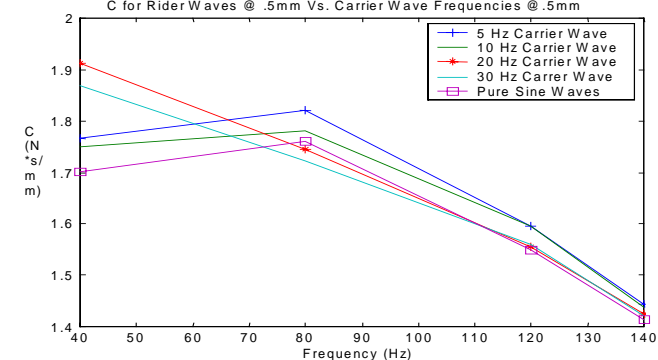


Figure 19: Effect of Carrier Wave Frequency on .5mm Rider Wave Damping Estimates

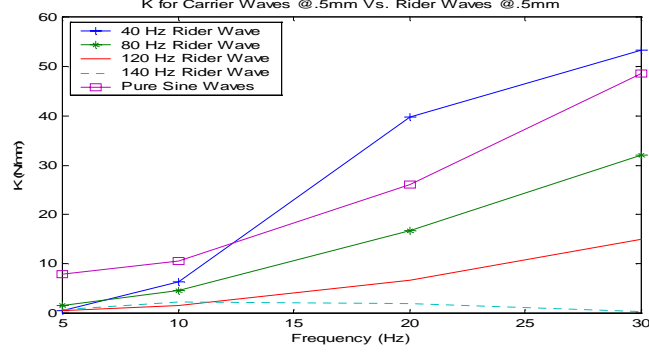


Figure 23: Effect of .5mm Rider Waves on Carrier Wave Stiffness Estimates

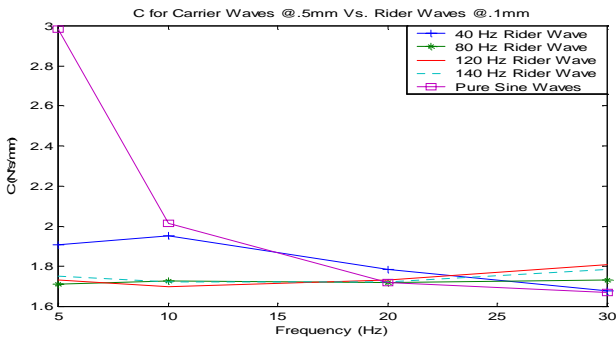


Figure 24: Effect of .1mm Rider Waves on Carrier Wave Damping Estimates

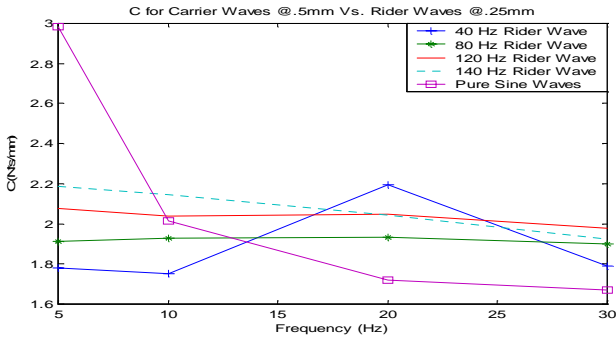


Figure 25: Effect of .25mm Rider Waves on Carrier Wave Damping Estimates

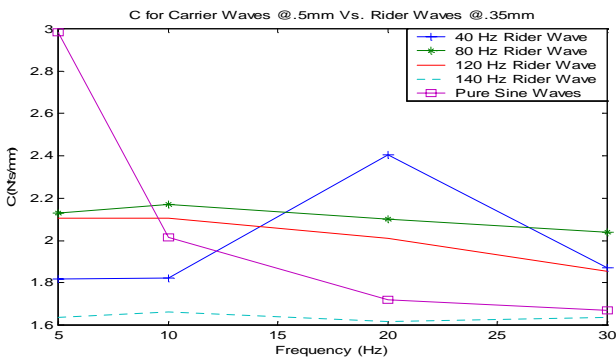


Figure 26: Effect of .35mm Rider Waves on Carrier Wave Damping Estimates

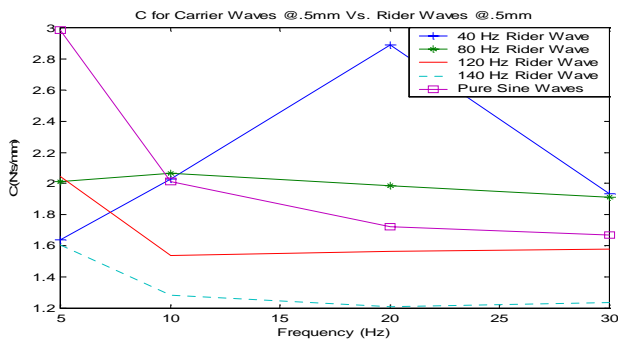


Figure 27: Damp Effect of .5mm Rider Waves on Carrier Wave Damping Estimates

## MULTIPLE FREQUENCY INPUT EXCITATION

Now that sine-on-sine input excitation has been examined, the next step is to determine these parameters when all frequencies of interest are present in the input excitation. It was decided to use random signals with the same envelope as the previously tested sine waves. For this study the peak-to-peak values of the random excitation was 1mm. This value was decided because there are pure sines with the same peak-to-peak values and because it yields the best signal to noise ratio of the available sine input amplitudes. Random signals are generated in three different ways for this study. The first random signal generated has constant amplitude for all frequencies. The second type of random signal generated weights the amplitudes at  $\frac{1}{f^1}$ . The final type of random signal

weights the amplitudes at  $\frac{1}{f^2}$ . It is important to

remember that the peak to peak values of all three of these random signals is 1mm. This does mean however, that the amplitude at a given frequency changes from drive file to drive file. The power spectral densities of the input displacement and the output force of these three signals can be seen in the Figure 28. The analysis of these signals is done spectral line by spectral line. The results of stiffness and damping estimates are shown in Figures 29 and 30. Examining the damping estimate first, it is noticed that above 60 Hz the damping estimates resulting from the input signals of  $\frac{1}{f^0}$  and

$\frac{1}{f^1}$  fall very close to the pure sine estimates. The estimates from  $\frac{1}{f^2}$  in the same region are higher than

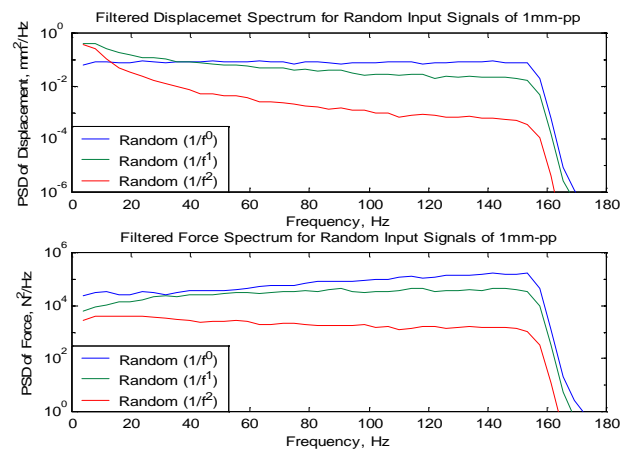


Figure 28: Power Spectral Densities of Input Displacement and Output Force for Random Input Signals

the pure sine estimates. Below 60 Hz none of the random signals show a good agreement with the pure sine values. One other thing noted is the fact that the estimates from  $\frac{1}{f^0}$  and  $\frac{1}{f^1}$  weighted random excitations are about the same throughout the entire frequency range. This phenomenon holds true for the stiffness estimates as well. Just like the damping estimates, the results from  $\frac{1}{f^2}$  weighting are higher than the other two, while the  $\frac{1}{f^0}$  and  $\frac{1}{f^1}$  weighted results are very close to one another. The results of stiffness for  $\frac{1}{f^0}$  seem to be an accurate estimator of the pure sine values above 70 Hz and below 20 Hz. Between 20 and 70 Hz the estimates are higher than the pure sine estimates. One alarming thing shown in the stiffness graphs is that the estimates resulting from  $\frac{1}{f^0}$  and  $\frac{1}{f^1}$ , below 60 Hz, fall

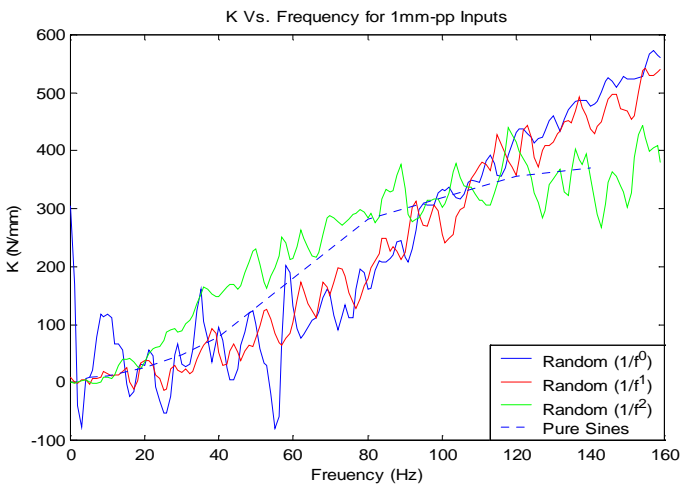


Figure 29: Stiffness Vs. Frequency for Random Input Signals compared to Pure Sine Values

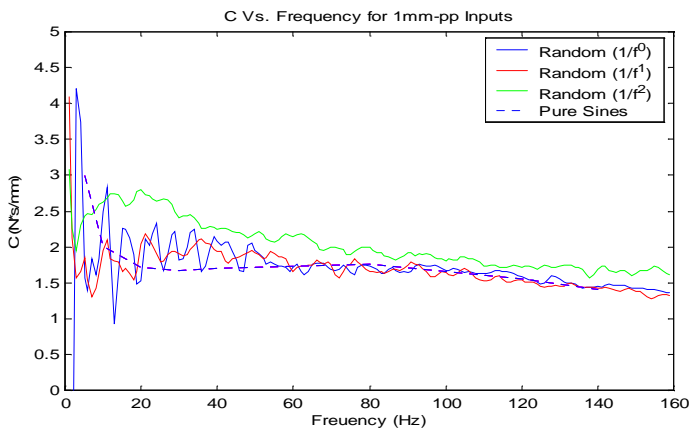


Figure 30: Damping Vs. Frequency for Random Input Signals Compared to Pure Sine Values

below zero. Having a negative stiffness in a shock absorber is not a possible situation.

As can be seen in Figure 31, the phase below 60 Hz rises above 90 degrees. This results in the stiffness estimates in these areas to be negative. The reason is that  $K = K^* \cos(\Phi)$ , and the cosine function changes

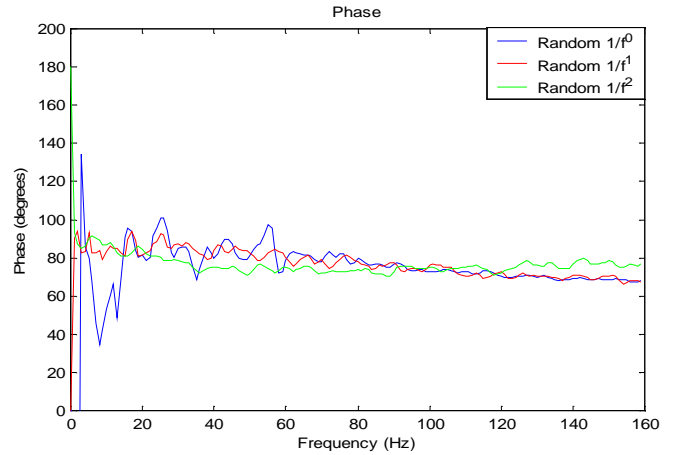


Figure 31: Phase between Input Displacement and Output Force for Random Inputs

sign at 90 degrees. It was hypothesized that the phase jumps were being caused by the shock absorber being over driven, by the amount of energy input at the higher frequencies. This was speculated because the

amplitude, for random  $\frac{1}{f^0}$  weighting, is the same at all frequencies. It is known that this is not the case when the shock absorber is in operation. In order to test this hypothesis the random input excitation of  $\frac{1}{f^0}$  was

filtered to contain only frequencies below 60 Hz. The shock absorber was then excited using this lower frequency limited random signal. As can be seen in Figure 32, the phase angle between input displacement

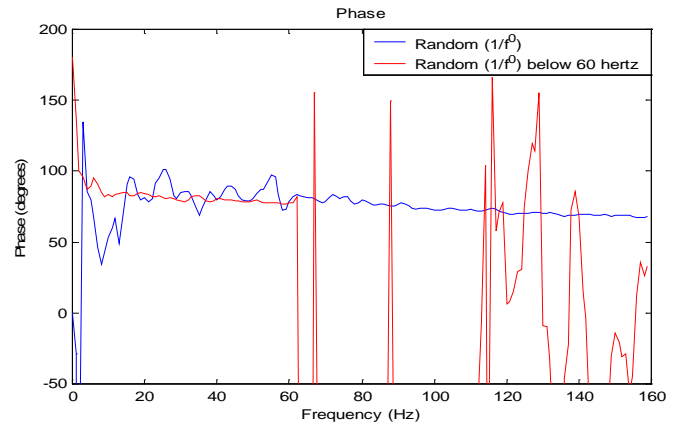


Figure 32: Comparison between Phase Values of  $1/f^0$  Random Signals

and output force, of this abbreviated random does not contain any jumps in phase like the broader frequency excitation. This supports the hypothesis that when all the frequencies are excited with the same, or close to the same amplitude, it is not a realistic situation and the shock absorber is being over driven.

As shown in Figure 33, the stiffness estimates became realistic for the abbreviated  $\frac{1}{f^0}$  random signal as

expected. The stiffness estimates from this filtered input signal fall close to the pure sine estimates. The two almost lie on top of each other below 60 Hz. The stiffness estimates looked very promising for obtaining the same parameter estimates with broadband noise as pure sine waves. However, when examining the damping estimates, in Figure 34, the same phenomenon does not hold true. The damping estimates obtained from the random signal, below 60 Hz, do not have the same estimates as obtained from the pure sine waves. The estimates from the abbreviated random signal have higher damping estimates than the pure sine estimates.

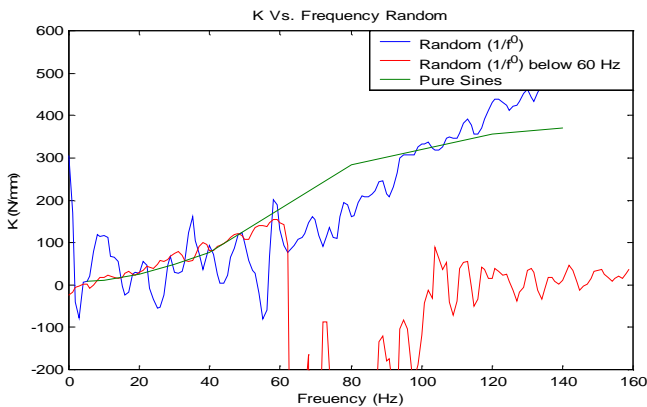


Figure 33: Comparison of Stiffness Estimates from Pure Sines and  $1/f^0$  Randoms

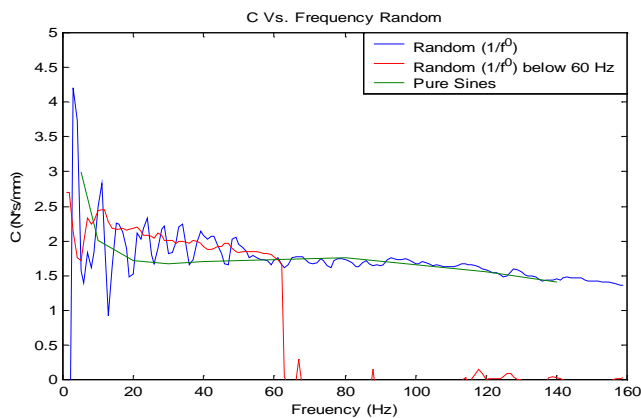


Figure 34: Comparison of Damping Estimates for Pure Sines and  $1/f^0$  Random Input

**CONCLUSIONS FROM BROADBAND RANDOMS** - What has been learned from the random noise excitation study of the shock absorber? If the shock absorber is not being over driven, the random excitation will result in believable estimations for both stiffness and damping. The results vary somewhat with the values obtained from pure sine excitation. However, there is no reason to assume that the baseline of the pure sine excitation yields the best estimations because in practice shock absorbers see broad band frequency inputs.

**ROAD EXCITATION**

In an effort to obtain a true shock absorber response in operation, a midsize sedan was instrumented with two 356 B08 PCB accelerometers. One accelerometer positioned on the top of the shock and one positioned was on the bottom of the shock. The automobile was then driven down a smooth highway, a semi rough paved road, and a rough dirt road, while the time traces of the accelerometers were recorded using the LMS Road Runner acquisition system. The difference between acceleration signals was integrated twice in the frequency domain, to get displacement. The signals were filtered below 2.5 Hz and above 160 Hz. The roughest dirt road profile is shown in Figure 35.

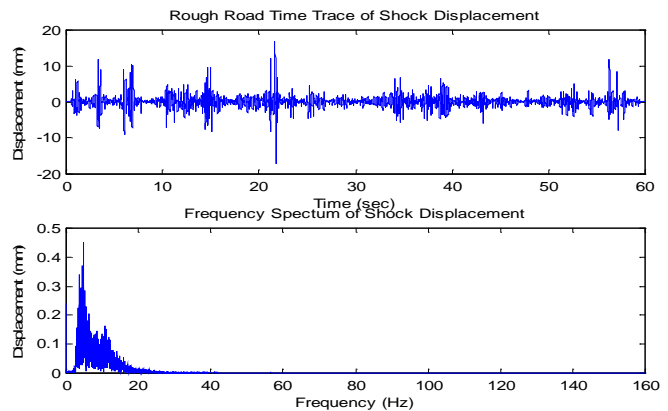


Figure 35: Measured Rough Road Profile

The time trace shows maximum displacements of about 14mm. The frequency domain representation of the road profile is quite interesting. The maximum displacements are about .45 mm and occur around 5 Hz. The displacement inputs, above 80 Hz, are miniscule compared to the displacement inputs at the lower frequencies. Due to dynamic range limitations on the MTS 831 machine these higher frequency lower amplitude signals are difficult to reproduce. This results in a low confidence level in the parameters estimated above 80 Hz. Shown in Figures 36 and 37, are the estimated shock absorber parameters from a road profile excitation. It is seen that the estimations do not look very realistic. The estimations for stiffness drop below 0, and the damping estimates are all over the place. The reason these estimates look like this may be due to the

reproduction of the road profiles in the MTS 831 machine.

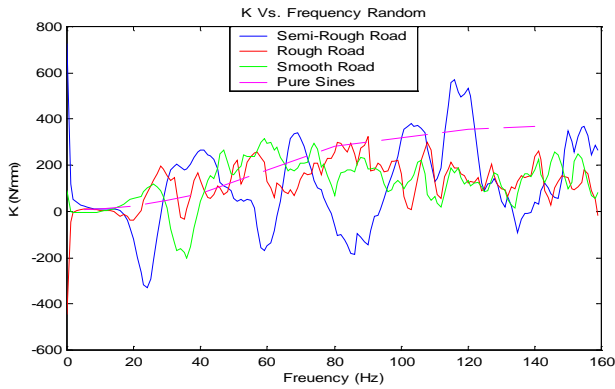


Figure 36: Stiffness Estimates Using the Road Data as Input

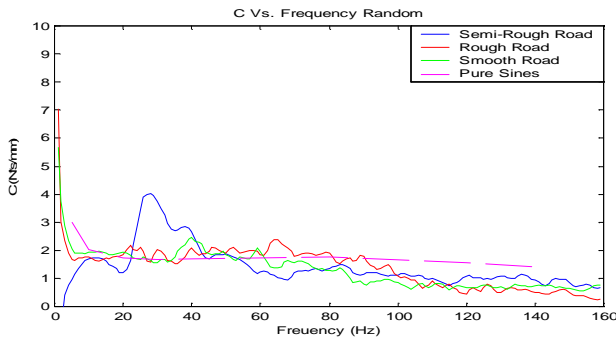


Figure 37: Damping Estimates Using the Road Data as Input

It is also possible that a different averaging scheme should be used when calculating the frequency response between the input displacement and the output force of the road excitations. The reason has not yet been determined. However, what has been done is to copy the frequency displacement spectrum and add a random phase to it. This yields a shaped random signal with the same frequency spectrum as the original road data. This is illustrated in Figure 38, where it is seen that the frequency spectrum is the same as Figure 35. However,

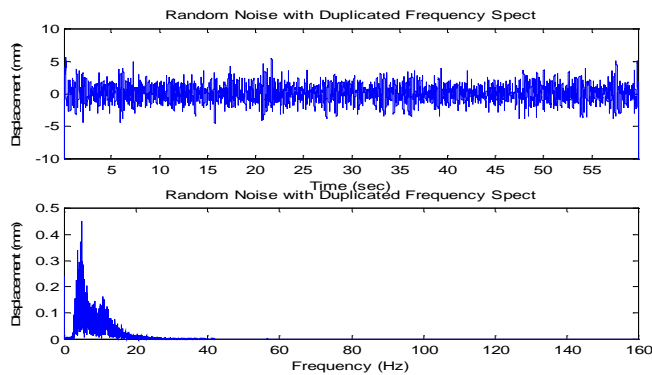


Figure 38: Duplicated Frequency Spectrum with Random Phase

the time signal is a random signal with the same spectral content as the measured road data.

Shown in Figures 39 and 40 are the estimated parameter results from the shaped road frequency spectrum random excitation. It is important to keep in mind that there is little confidence in these results above 80 Hz, due to the low amplitudes. The stiffness and damping curves are much more realistic for an automotive shock absorber using this method as opposed to the pure road response excitation. In the area in which confidence is held the parameter estimations are very close to the estimations from pure sine wave excitation. There are slight deviations between the two methods, but one must keep in mind that the road parameters are estimated at many more frequencies than the pure tones. Due to the realistic displacement conditions during this test, the results are as close to how the shock acts in operation as can be done at this time. In an effort to smooth these graphs out, they have been curve fit in Matlab.

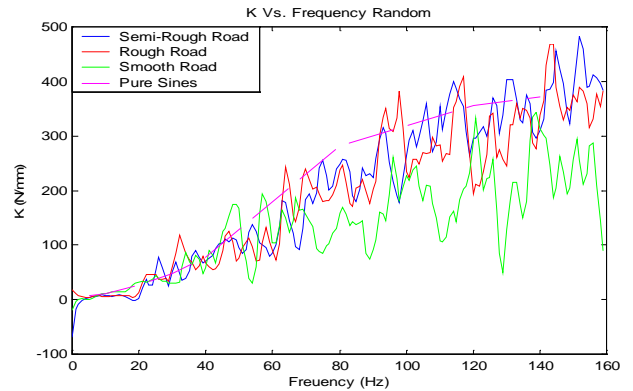


Figure 39: Stiffness Estimates using road data with random phase

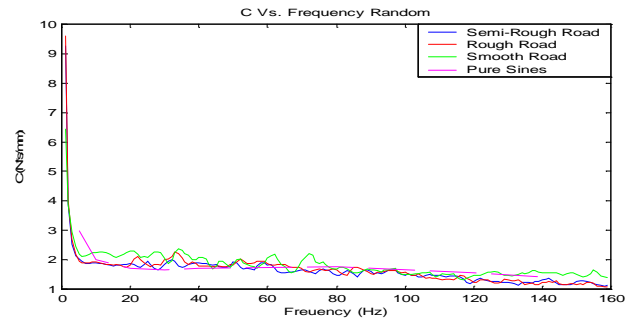


Figure 40: Damping Estimates using road data with random phase

The results are shown here in Figures 41 and 42. It is seen that the stiffness and damping estimate are fairly close to those of pure sine waves. In the case of stiffness the estimates are a little lower than those obtained with pure sine excitation. The smooth road stiffness estimations fall well below the pure sine

estimations and the other road profile estimations. This is believed to be a result of the reproduction of the small displacements seen on the smooth road. Therefore, this series is disregarded because the data is approaching the noise floor of the measurement system. The two other road profiles are very close to one another and are of higher amplitudes, so these results are meaningful. The damping estimates using the shaped road spectrum fall almost on top of the estimated damping from pure sine excitation.

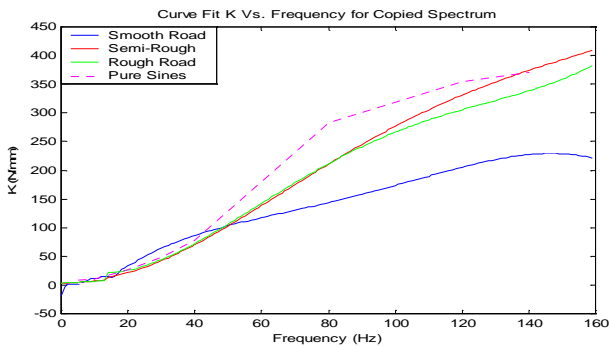


Figure 41: Stiffness Vs. frequency from copied road spectrum curve fit

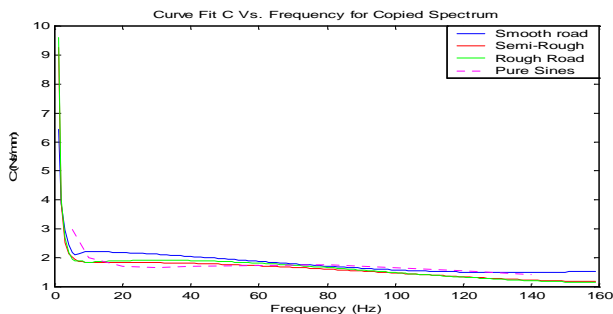


Figure 42: Damping Vs. Frequency from copied road spectrum curve fit

## CONCLUSIONS

The results of these studies have proven a number of things. First it has proven that when a comparison study is being done on an automotive shock absorber the temperature of the shock absorber must be maintained and monitored throughout the test. Another thing that must be monitored is the stroke length of the shock absorber from test to test, if the estimated parameters are going to be compared.

Secondly, when two sine waves are added together and used to actuate a shock absorber, the parameters estimated at each frequency are dependent on one another. The dependency is a function of the amplitude of the two waves and a function of how far apart the two frequencies are. In the case where one frequency is

quite a bit higher in frequency than the other, the higher frequency maintains its parameters where as the lower frequency parameter estimations are very low.

The parameters estimated using sine-on-sine testing were not the same as the parameters estimated using pure sine waves. This infers that maybe pure sine excitation does not yield good parameter estimations. However, when broadband excitation was used the parameters estimated were very close to the estimations using pure sine waves. This means that the pure sine excitation produces realistic estimated parameters. It has been shown in the discourse of this paper that all the estimated parameters can be found at once when using a shaped random signal. The best type of shaped random is one that has the same frequency spectrum that the shock absorber sees in practice. When using this type of shaped random signal, the parameters estimated are close to those estimated using pure sine excitation. Using this type of excitation has a couple of big advantages. First the actual test takes far less time than the stepped sine sweep. Also, due to the short test time, the temperature of the shock absorber does not change significantly during the test. The biggest advantage is that the dynamic parameters for all amplitudes and frequencies are obtained simultaneously. At this time some of the higher frequency and very small amplitude road responses cannot be reproduced, but this problem is sure to be addressed and solved in the not too distant future.

## REFERENCES

1. Rao, M. D., Gruenberg, S., and Torab, H., "Measurement of Dynamic Properties of Automotive Shock Absorbers for NVH," Proc. Of SAE 1999 Noise and Vibrations Conf. 1999, pp. 1433-1438.
2. Cafferty, S., Worden, K., Tomlinson, G., "Characterization of Automotive Shock Absorbers Using Random Excitation," Proc. Instn. Mech Engrs, Vol 209, 1995.
3. Belingardi, G. and Camoanile, P., "Improvement of the Shock Absorber Dynamic Simulation by the Restoring Force Surface Mapping Method," Proc. Of the 15<sup>th</sup> International Seminar on Modal Analysis and Structural Dynamics, Leuven, Belgium, pp.441-454, 1990.
4. Duym, S., Schoukens, J., Guillaume, P., "A Local Restoring Force Surface Method," Proc. 13<sup>th</sup> IMAC, Nashville, Tennessee, pp. 1392-1399, 1995.
5. Lang, H. H., "A Study of the Characteristics of Automotive Dampers at High Stroke Frequencies," Ph.D. Thesis, University of Michigan, 1977.
6. Morman, K., "A Model for the Analysis and Simulation of Hydraulic Shock Absorber Performance, Part I- Theoretical development (SR-83-043), Part II- Parameter Identification and Model Validation Studies (SR-86-61), Ford Motor Company Research Staff Reports.
7. Reybrouck, K., "A Non Linear Parametric Model of an Automotive Shock Absorber," SAE Paper No. 940869, Vehicle Suspension and System Advancements, SP-1031, pp. 79-86, 1994.
8. MTS TestStar II Control Manual, 790.31 Dynamic Characterization.
9. Surace, C., Storer, D., Tomlinson, G. R., "Characterizing an Automotive Shock Absorber and the Dependence on the Temperature," Proc. of 10<sup>th</sup> IMAC, 1992, pp. 1317-1326.

